GEOPHYSICAL INVESTIGATIONS OF SEISMICALLY INDUCED SURFACE EFFECTS: CASE STUDY OF A LANDSLIDE IN THE SUUSAMYR VALLEY, KYRGYZSTAN

H.-B. HAVENITH[1], D. JONGMANS[1], K. ABDRAKHMATOV[2], P. TREFOIS[3], D. DELVAUX[3] and I.A. TORGOEV[4]

[1]*Laboratory of Geophysics, University of Liege, 4000 Liege, Belgium (E-mail: HB.Havenith@ulg.ac.be);* [2]*Kyrgyz Institute of Seismology, 720815 Bishkek, Kyrgyzstan;* [3]*Department of Geology, Royal Museum of Central Africa, 3080 Tervuren, Belgium;* [4]*Kyrgyz Academy of Sciences, 720815 Bishkek, Kyrgyzstan*

(Received 5 July, 1999; Accepted 22 June, 2000)

Abstract. In summer 1998, a geophysical survey including seismic profiles and electrical tomography has been carried out in the Suusamyr valley, Kyrgyzstan. The scope was to investigate surface effects induced by the Ms = 7.3 Suusamyr earthquake, the 19th of August, 1992. In this paper, special attention is paid to the case study of a debris slide triggered by the earthquake. Seismic data are analysed by P-wave refraction technique and by surface wave inversion. Electrical tomographic profiles are processed by 2D-inversion.

Using geotechnical and geological information, P-velocity models and resistivity sections are interpreted in terms of geological materials, in order to build a geological 3D model. On the basis of the latter, we carried out static finite element computations as well as static and pseudo-static calculations with Janbu's method. Newmark displacement was computed, considering or not the influence of the shallow soft deposits. The results are compared to the real displacement observed in the field and conclusions are drawn about the mechanism of the landslide.

Keywords: landslide, Suusamyr earthquake, electrical tomography, seismic profiles, finite element modelling, stability analysis.

1. Introduction

Advanced modelling of slope stability is directly dependent on the precise knowledge of the sub-surface geology. In this regard, intensive prospecting of instability processes may play an important role for the local hazard assessment (Hoek and Bray, 1981).

In general, detailed investigations of landslides for back-analysis calculations include geotechnical tests in situ and in the laboratory, but there is often a need to apply geophysical methods to provide additional data on the sub-surface geology. The relatively rapid acquirement of information over large areas up to a depth of several tens of meters turns geophysical prospecting into an important complementary tool for the investigation of landslides (McCann and Forster, 1990).

The geophysical prospecting also becomes an essential technique when the field conditions for the realisation of boreholes or penetration tests are difficult,

Surveys in Geophysics **21:** 349–369, 2000.

as in high mountain regions. This is the case for the present study realised in Kyrgyzstan, Central Asia (Figure 1), in the Tien Shan range. The field experiment combined geophysical, geotechnical and geological investigations and was focused on landslides and surface effects in the Suusamyr valley, induced by the Ms = 7.3 Suusamyr earthquake, the 19th of August, 1992 (Figure 1b). This earthquake triggered many landslides, the most disastrous one, a rock avalanche near the village of Toluk on the southern flank of the Suusamyr range, killed about 35 people. In total, the earthquake caused about 50 casualties (Bogachkin et al., 1993; Ghose et al., 1997).

In the target area, the Chet-Korumdy ridge, several old reactivated and newly formed landslides affected the Bishkek-Osh highway (Figures 2a and 2b). Other seismically induced surface effects such as mud volcanoes, surface ruptures, cracks and fissures were also observed along this highway.

Before presenting the case study of one landslide and two examples of geophysical investigations on the induced surface effects, we will briefly describe the geological and tectonic setting of the region.

2. Seismo-Tectonic Context of the Tien Shan

The Tien Shan is a high, intracontinental mountain belt in Central Asia, with an east-west extension of about 2500 km and a maximum width of more than 500 km. It culminates in the 7453 m high Peak Pobedi in Eastern Kyrgyzstan.

The Kyrgyz Tien Shan is delimited in the North by the stable Kazakh platform and in the South by the Tarim basin (Avouac et al., 1993, Figure 1b). The structure of the Tien Shan is characterised by alternating, roughly east-west trending, mountain ranges and intramontane basins. Palaeozoic rocks and older basement constitute the core of the ranges, whereas the basins are filled by Cenozoic and some Mesozoic sediments and are mostly bounded by oppositely vergent thrust faults (Cobbold et al., 1994). Another structural feature are strike slip faults, the most prominent one being the NW-SE trending Talas-Fergana fault (Figure 1b) with a total dextral offset, since Permian times, of about 200 km. Thrust and strike slip faults accommodate a yearly shortening of 10-30 mm (Abdrakhmatov et al., 1996, Reigber et al., 1999) throughout this intracontinental mountain belt.

Due to its tectonic activity, the Tien Shan is prone to a high seismicity. In the last century, several strong earthquakes struck the region (Figure 1b), like the M = 8.2 Kemin earthquake in 1911, the M = 7.6 Chatkal earthquake in 1946 or the Ms = 7.3 Suusamyr earthquake in 1992 (Mellors et al., 1997; Gomez et al., 1997).

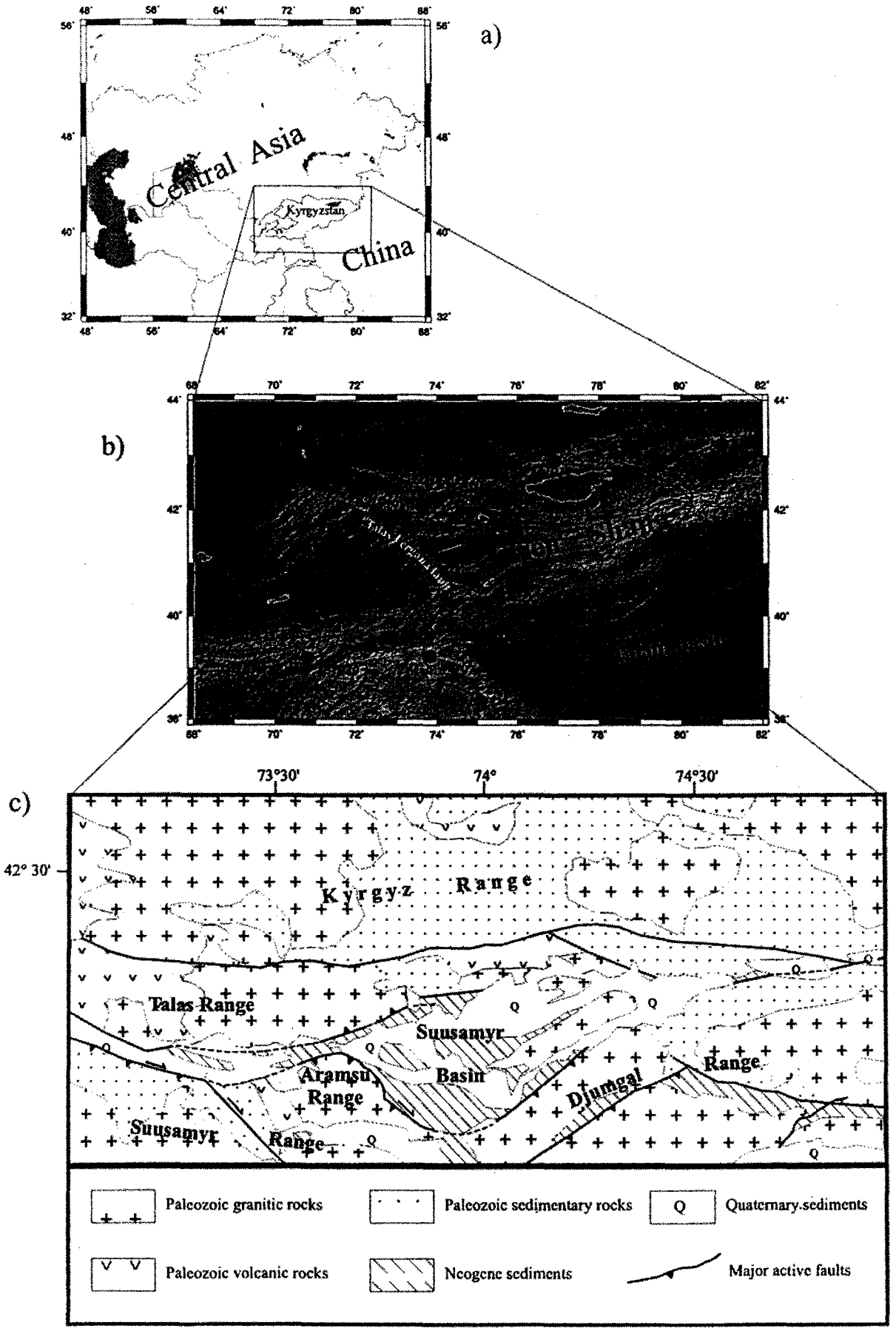

Figure 1. (a) Location of Kyrgyzstan. (b) Map showing the morphology of the Kyrgyz Tien Shan and epicenters of largest historical earthquakes ($M > 7.1$). (c) Geological map of the Suusamyr basin and the surrounding Kyrgyz, Talas, Suusamyr, Aramsu and Djumgal ranges (modified from the Geological map of Kirghiz SSR, 1980).

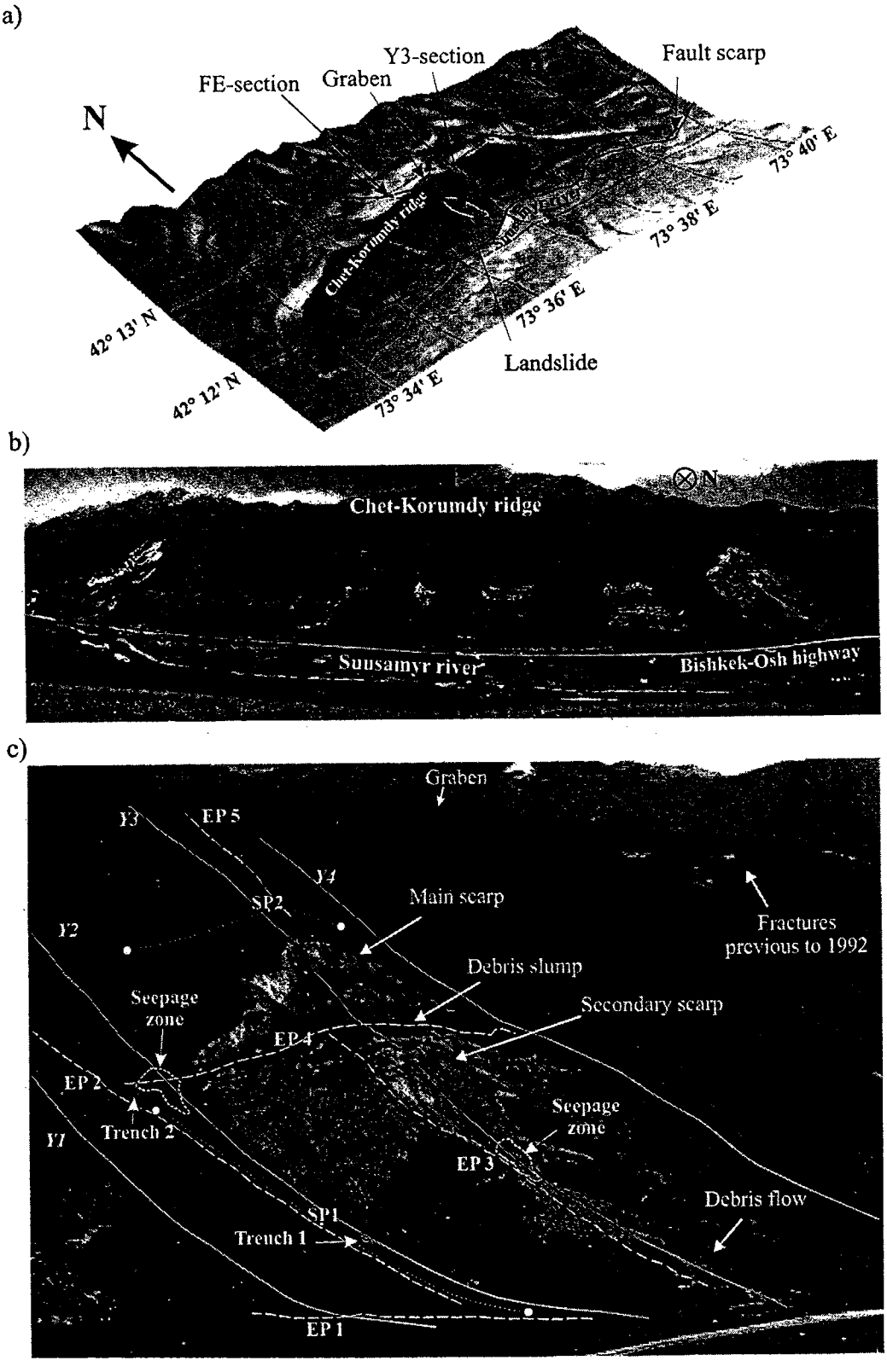

Figure 2. (a) Digital elevation model of the Chet-Korumdy ridge performed based on georeferenced 1/25000 topographical maps (previous to 1992). Localisation of the investigated sites: the Suusamyr landslide, the graben and the fault scarp. The indicated FE- and Y3-sections correspond respectively to the profiles used for FE-modelling and for pseudo-static slope stability computations. (b) Surface effects on the south-facing slope of the Chet-Korumdy ridge triggered by the Ms = 7.3 Suusamyr earthquake in 1992, the mass movement to the left is an old reactivated landslide. (c) Detailed view on the investigated landslide showing electrical profiles (EP) and seismic profiles (SP), Y1–Y4 sections (see also Figure 4) and two trenches are indicated. The position of the direct and reverse shots of the seismic profiles are marked by a white dot.

3. Geological Setting

The Suusamyr basin is located in the northern part of the Tien Shan, among the Kyrgyz, Talas, Suusamyr, Aramsu and Djumgal ranges (Figures 1b and 1c). As most intramontane basins in the Tien Shan, it is bordered on both sides by active oppositely vergent thrust faults. The surrounding ranges are made by Ordovician-age granitic plutons, while the basin itself is mainly filled by Neogene sediments, sands and clays, of lacustrine origin (Geological map of Kirghiz SSR, 1980, Figure 1c). Inside the basin, young anticlinal ridges cored by steeply dipping Neogene sediments, like in the Chet-Korumdy ridge, formed as the result of the migration of the thrusting towards the interior of the basin (Ghose et al., 1997). In most parts, the Neogene sediments are overlaid by Quaternary deposits clearly affected by late-Pleistocene-Holocene tectonics and seismic activity (Korjenkov et al., 1999). In the Chet-Korumdy ridge, the latter consist of reddish arenites of fluvio-glacial origin, produced by the weathering of Talas range grantic rocks.

4. Ground Surface Effects of the 1992 Earthquake

During the 1992 Suusamyr earthquake, landslides as well as other ground failures were triggered on the south-facing slope and on the crest of the Chet-Korumdy ridge (Figure 2). The landslides can be classified as debris slumps, debris flows or may present a combination of these two types of movements. In addition, fresh scarps were observed on old landslides, which indicate their recent reactivation in 1992.

Our case study was focused on the largest, newly formed landslide (Figure 2c), of a volume of 0.5–1 $\times$ 10^6 m^3, which we will call the Suusamyr landslide in the following. In its upper part, below the 50 m high main scarp, the landslide consists of a multi- rotational debris slump. Several secondary scarps formed on the body of the slump due to the lateral spreading of the debris material that turned into a debris flow in the lowest part of the landslide.

Besides the other smaller landslides presenting a less complex structure, different fracture patterns affect the southern slope of the ridge (Figure 2c). Several of them have been observed on air-photographs prior to the 1992 earthquake and are therefore not related to this event. At the crest of the ridge, a gravitational graben, 10 m wide and extending over more than 100 m along the crest, formed during the earthquake between a main south-facing and secondary north-facing scarps. North of the crest, no significant surface effects have been detected.

At the bottom of the Suusamyr valley, surface faulting related to the 1992 earthquake formed several scarps in alluvial deposits, the main fault scarp being up to 2.5 m high and 500 m long (Figures 2a and 4). The distance between the above-mentioned landslides and the fault scarp is less than 5 km (Figure 2a).

5. Geophysical Exploration Methods

During a geophysical campaign in summer 1998, seismic refraction tests and electrical tomography were applied on the 1992 earthquake-induced surface effects in the vicinity of the Chet-Korumdy ridge. The prospecting chiefly aimed at the determination of the structure of the above-mentioned Suusamyr landslide (Figure 2c), in order to constrain back-analysis calculations. Parallel to this main survey, electrical tomography was also applied to investigate the sub-surface structure of the gravitational graben at the top of the hill and of the major fault scarp at the bottom of the valley.

Near to the debris slide, two 250 m long seismic refraction profiles (Figure 2c) were carried out with twenty-four 4.5 Hz geophones spaced by 10 m and connected to a 16 bit seismograph. Explosives were used as source for the direct and the reverse shots. The seismograms were analysed with regard to the refraction of P-waves in order to define the slope structure in terms of P-wave velocity (Vp) models. During an earthquake, the ground motions may be strongly amplified by local geological conditions (Aki, 1993) and these effects are mainly controlled by the shear wave velocity values of the different formations. Vertical S-wave velocity profiles were deduced from the analysis of the surface waves recorded during the refraction tests. The surface wave inversion technique (Herrmann, 1987) using the dispersive properties of these waves was applied to determine the S-wave velocity and quality factor (Qs) values of the constituting layers.

Electrical tomography survey was performed using the ABEM Lund Imaging system (Dahlin, 1996) with a Wenner configuration. On and around the landslide, the survey included five, 200–315 m long, geoelectric profiles (Figure 2c) with 41–65 electrodes spaced by 5 m. The electrical tomography profiles across the graben and the fault scarp (Figures 2a, 4 and 5) were composed of 41 electrodes spaced by 2 m. The data were processed with the 2D-inversion algorithm proposed by Loke and Barker (1996) to obtain a resistivity section. According to the profile length, the investigation depth was between 30 and 40 m. The penetration depth along the closer spaced profiles across the graben and the scarp was about 12 m.

In order to calibrate the geophysical data and to determine the geotechnical parameters of the geological units, two 2.5 m deep trenches have been dug 100 m to the West of the landslide (Figure 3b). In total 15 samples, taken from the 2 trenches (along the westernmost geoelectric profile EP2, Figure 2c and 3b), were analysed for grain size distributions, water content and static shear strength.

6. Results of the Geophysical Investigation of the Landslide

The reconstruction of the shallow geological structure was performed using Vp-models and resistivity sections. On Figure 2c are located the Vp models at the extremities of two profiles (beneath the direct and the reverse shots). The sub-

TABLE I

Geological units, seismic and electrical parameters

Layer	Material	*P*-wave velocities (m/s)	Resistivity (Ωm)
1a	High resistivity arenites/soil	410-540	>380
1b	Medium resistivity arenites	174-380	
1c	Low resistivity arenites	1150-1540	70-175
2a	Silty clays	1840-2110	25-70
2b	Low resistivity silty clays		<25
3	Neogene sediments	3100-3390	–

surface geology is defined by 4 seismic layers with Vp ranging from 500 m/s near the surface up to 3300 m/s in the bedrock at 45m to 60m depth (Table I). The electrical characteristics of the surrounding geology were obtained by 2D-inversion of the geoelectric profiles (Figure 2c). The principal factors influencing the ground resistivity are the nature of the material and the water content. Regarding these properties, a resistivity section may provide a valuable information on the subsurface geology.

In Figure 3 are presented three geoelectric sections that permitted to define the structure of the landslide. The first electrical tomography (EP4 in Figure 2c) crosses the debris slump, just below the main scarp. The resistivity values displayed on the section range from less than 20 Ωm to over 1000 Ωm (Figure 3a). The high resistivity zone in the central part of the section outlines the body of the debris slump. At the edges of the slide the lateral changes of resistivity correspond in the field with a seepage zone in the West and with a lateral scarp in the East (Figure 3a and 2c). Though, a vertical change of resistivity can also be observed, the base of the slump may not be defined from this single section without any calibration of the resistivity data. Therefore resistivity values displayed on the geoelectric profile EP2 were compared with observations in two trenches located along this profile (Figure 3b). The lithologies vertically exposed in the trenches were dry soil, arenites and silty clays. The latter cropped out only in the lower trench (trench 1). At the interface between the silty clays and the overlying arenites a contact zone marked by small slip surfaces was observed. On section EP2, this interface corresponds approximately to the 70 Ωm contour line. This limit has then been used on all five geoelectric profiles to define the contact between resistive arenites and conductive silty clays. In fact, on section EP4, the light 70 Ωm contour line matches approximately with the lateral extent of the debris slump, which was observed to be mainly made of arenites. The depth of the landslide base was estimated at 40 m by extrapolation of the 70 Ωm below the penetration depth of 30 m (dashed line in Figure 3a).

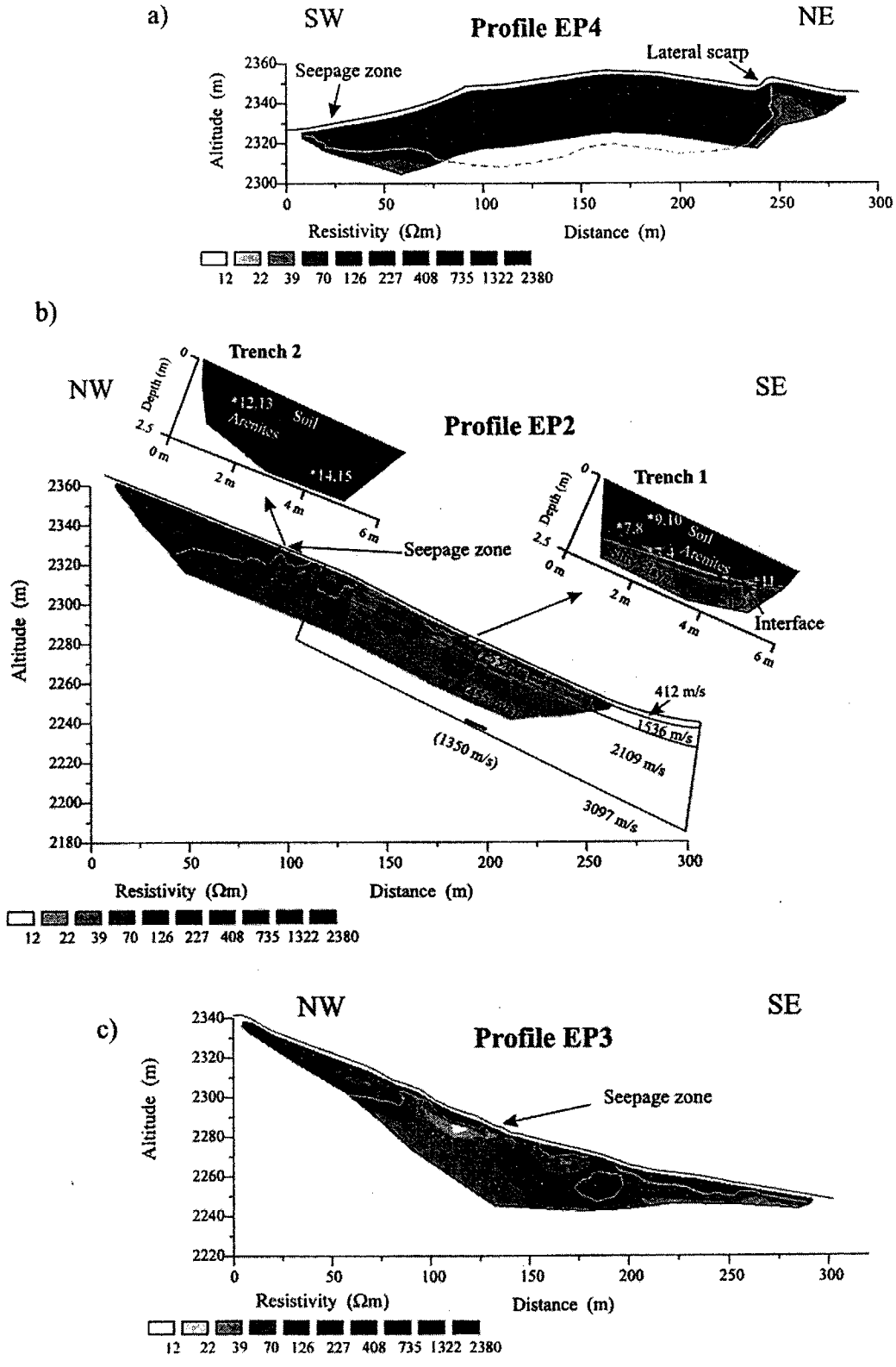

Figure 3. (a) Geoelectric profile EP4 across the upper portion of the debris slump. The light contour line (70 Ωm) indicates the approximate contact between arenites and silty clays, the dashed line corresponds to its extrapolation below the investigation depth. (b) Electrical tomography EP2 and seismic profile SP1 located at 100 m to the West of the landslide. Schematic view of the two trenches show the observed lithologies, the ground water level (trench 2), the position of the samples (stars) in the trench as well as the projection of the 70 Ωm contour line and its extrapolation (dashed) above the minimum investigation depth of 1 m. Along the seismic profile SP1 are indicated *P*-velocities and *S*-velocities (in brackets) of the layers. (c) Geoelectric section EP3 of the middle-lower part of the debris slump and debris flow and indication of the seepage zone.

The geoelectric profile EP2 (Figure 3b) displays in general lower resistivity values than section EP4. In the upper part, however, the resistivity increases, probably connected with a growing thickness of arenites towards the top of the slope. Also the upper trench (Trench 2 in Figure 3b) did not expose the silty clays. But waterlogged arenites at the bottom of the trench indicated the proximity of the more impermeable silty clays at depth. This observation fits with the trace of the 70 Ωm contour line on EP2 close to the bottom of the trench. In the lower part of the section, the seismic profile SP1 was projected on the EP2 profile. This allows to readily compare the P- velocities of the three first seismic layers with the resistivity data (see Table I for comparison). However, the deepest seismic layer with a P-velocity larger than 3000 m/s lies below the investigation depth of the electric tomography. Field observations in outcrops at the bottom of the valley indicate that the deepest seismic layer may correspond to Neogene sediments consisting in alternating, steeply dipping layers of very compacted sands and clays.

On the third geoelectric section (EP3 in Figures 2c and 3c), the 70 Ωm contour line defines approximately the base of the debris slump between 60 m and 125 m on the X-axis as inferred from the calibration of the resistivities in the trenches. Downhill, in the lower part of the landslide, the profile runs on the debris flow characterised by a heterogeneous resistivity distribution related to the presence of rill wash on the surface, inducing zones of lower resistivities in the arenites. Some water seepage has been observed at the bottom of the secondary scarp, probably indicating the shallow depth of the silty clays at this location.

From the geophysical results and the geological observations, three main layers were defined (Table I). The first layer corresponds to the arenites with a resistivity higher than 70 Ωm, while the deepest layers are the silty clays and the Neogene sediments. In terms of the geophysical properties the arenites are subdivided into three classes : high resistivity, medium resistivity and low resistivity arenites. The two first types of arenites have a P-velocity of about 500 m/s, the latter has a P-velocity of more than 1100 m/s. Silty clays are subdivided into silty clays and low resistivity silty clays, both with a P-velocity of about 2000 m/s. The Neogene sediments could only be characterised by their P-velocity of more than 3000 m/s.

A simplified three dimensional 3-layer model of subsurface geology (Figure 3c) was reconstructed from the geophysical results, showing four longitudinal sections (Y1–Y4) and four horizontal ones (X1–X4). The longitudinal Y3-section (Figures 2c and 4) displays the principal features of the landslide: main scarp, secondary scarp, debris slump and the debris flow. It clearly shows a larger thickness of arenites (about 40 m) in comparison to the adjacent sections Y2 and Y4 (2–25 m). The section Y1, located on an old landslide, also shows a large thickness of arenites that diminishes from 25 m at the crossing with X2 to 2 m at the intersection with X1. For all Y sections in general, the thickness increases towards the top of the slope as shown by the geoelectric profile EP2 (Figure 3b). This result is also validated by the resistivity profile EP5 above the landslide (see Figure 2c for location), which does only display resistivity values higher than 70 Ωm (up to a depth of

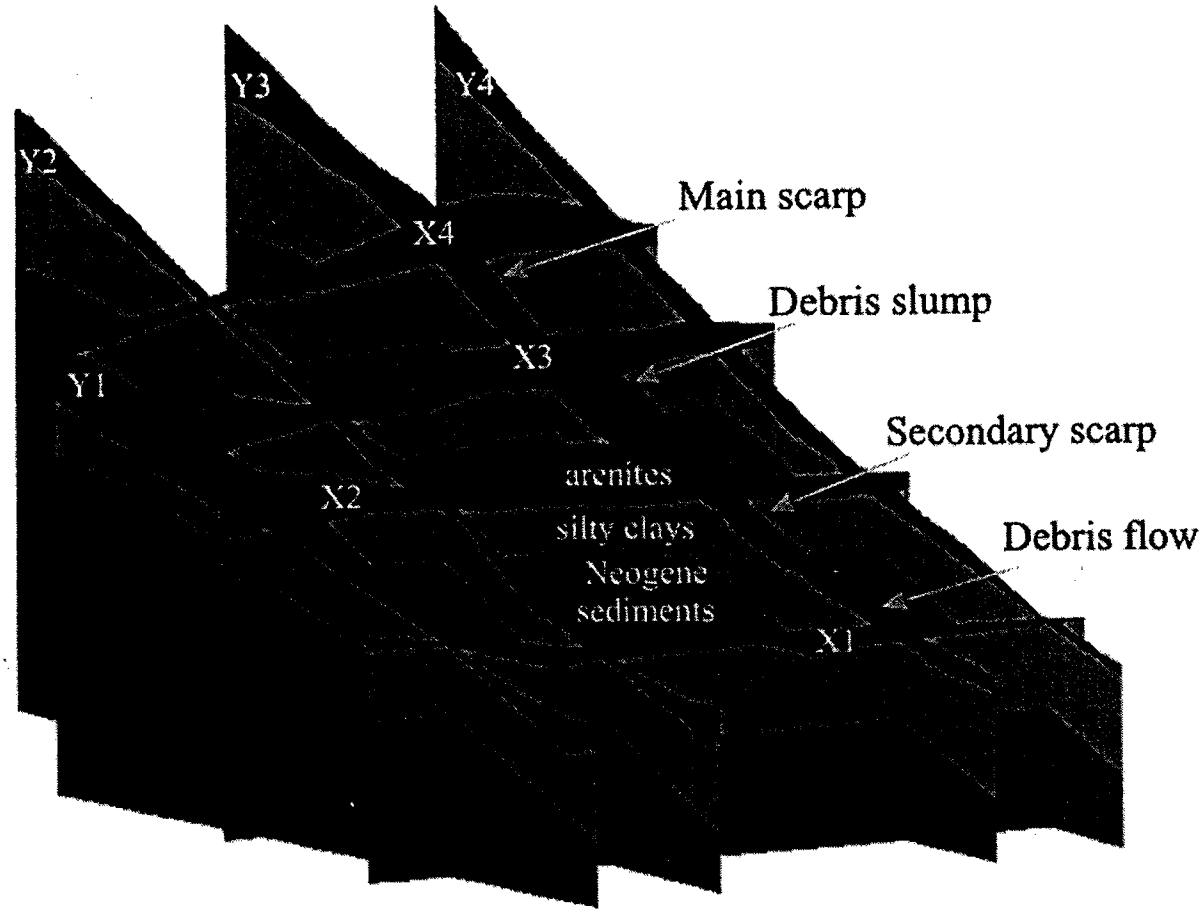

Figure 4. Three-dimensional 3-layer model showing the subsurface geology of the landslide (see Figure 2 for location).

30 m). Accumulations of arenites can also be observed in the lowest portion of the sections Y1 and Y2, as evinced from the geoelectric profile EP1 at the foot of the slope (see Figure 2c for location). Along the X sections, the thickness of arenites generally grows below convex morphologies. In connection with the observation that most landslides on the southern slope of the Chet-Korumdy ridge triggered in 1992 affected convex topographies, an influence of the arenite layer thickness on the slope stability can be expected. The reason for this might be the oversteepened slope of existing arenite accumulations. The origin of these latter is the thick arenite layer at the crest of the ridge, while mass movements and rill wash account for the transportation. The latter also increases the slope of the accumulated masses and thereby the sliding hazard.

7. Geophysical Investigation of Surface Ruptures

A geoelectric survey was performed on two other types of surface effects. In particular, an electrical profile was executed across the main fault scarp at the bottom of the valley in order to investigate the fault geometry at depth. The location of the profile and the resistivity section are shown in Figure 5.

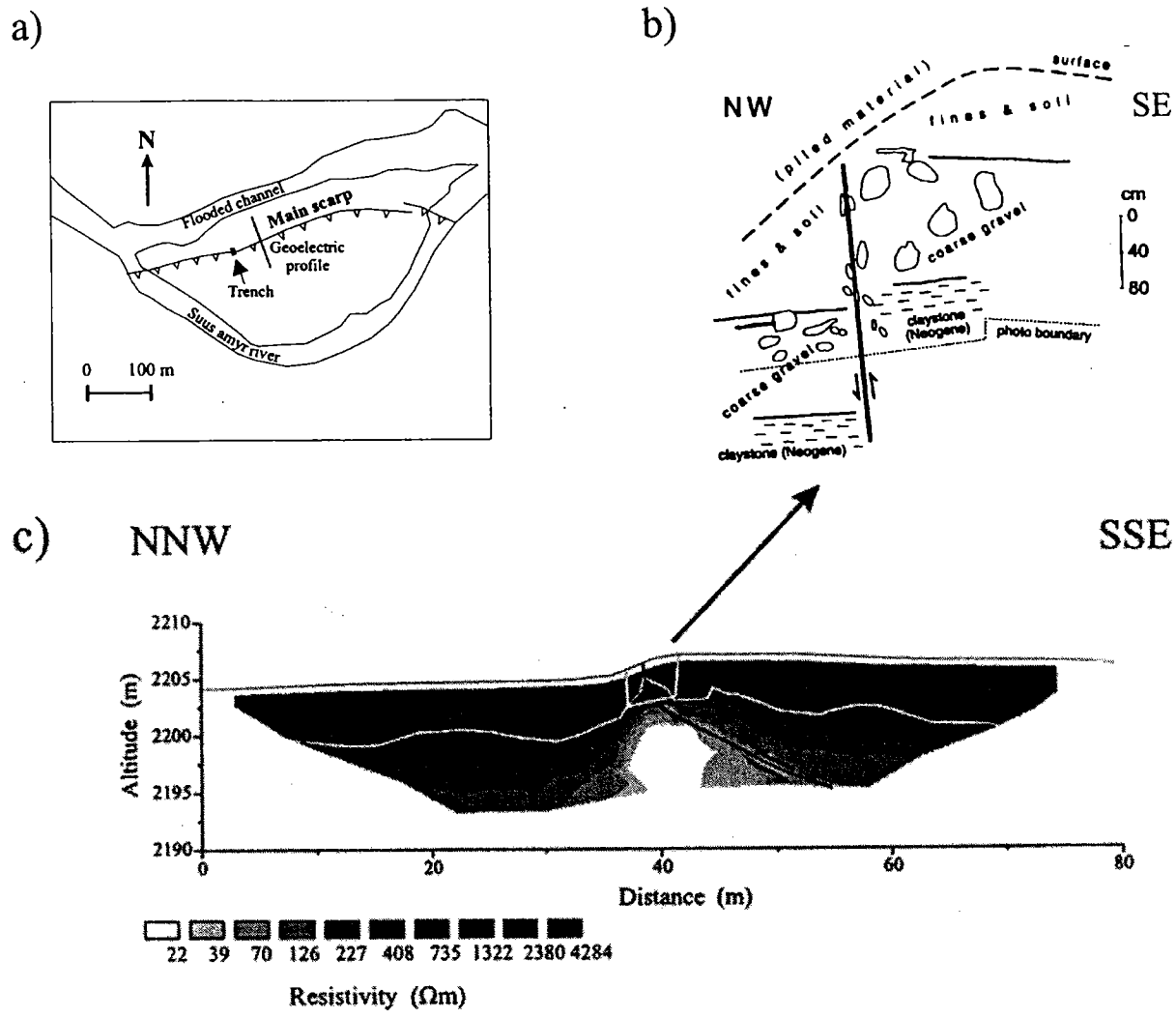

Figure 5. (a) Sketch showing the localisation of the geoelectric profile across the fault scarp and the trench made by Korjenkov et al. (1999). (b) Drawing of the fault observed in the trench (Korjenkov et al., 1999). (c) Resistivity section across the main fault scarp with indication of the inferred lithological contact (white line) between alluvial deposits (above) and Neogene sediments (below) and the fault mechanism.

A remarkable characteristic of the section is the large range of displayed resistivity values. Resistivities vary from less than 20 Ωm at depth to over 4000 ?m close to the surface. A trench made by Korjenkov et al. (1999) across the fault scarp allowed to calibrate the resistivity values (Figure 5b and 5c). The superficial high resistivities are related to alluvial deposits, mainly large boulders poorly cemented by silts or clays overlying the Neogene sediments. Due to the low ground water level in summer, the alluvial layer is dry and induces very high resistivities. The underlying layer is composed of claystone (Neogene) that shows similar electrical properties as the silty clays in the landslide site. The extreme resistivity contrast between the layers allows to readily distinguish different lithologies. However, the data inversion cannot reproduce the sharp spatial variation of the electrical properties. The observations in the trench made by Korjenkov et al. (1999) indicate that the contact between the layers can be located around the 1300 Ωm (light) contour.

Figure 5c reveals that there is a clear difference of altitude (about 1.5m) along the contour close to the fault scarp in relation to the thrusting of the southern block over the northern (Figure 5b, Korjenkov et al., 1999). In addition, the well defined lateral change of resistivity, near the surface at 39 m on the X-axis, coincides with the location of the fault trace in the trench. At depth, the resistivity-layers are disturbed just below the scarp, with dipping contour lines on both sides of the scarp.

The second supplementary investigation was conducted on the graben at the crest of the Chet-Korumdy ridge (Figures 2a and 6a). The resistivity section (Figure 6b) shows high resistivity values (>400 Ωm) at 3-7 m of depth, which correspond to the presence of arenites. Below the graben, a decrease of resistivities can be observed. Yet, without any calibration of the geophysical data, the interpretation of this feature is not straightforward.

8. Slope Stability Calculations

Geophysical data have been shown to provide important indications on geometrical and geophysical factors inducing instability. A quantitative back-analysis needs additional information such as geotechnical parameters of the involved lithologies. Most of the parameters (cohesion, friction angle, density) were obtained by simple shear-box tests and other laboratory tests performed on 15 samples from the two trenches (Table II, see Figure 3b for location of the samples). The range of values shown in Table II are peak shear strength values, because the applied method cannot determine the respective residual shear strength. Some of the indicated parameters values (E' and parameters for the Neogene sediments) were taken from references (Philipponnat, 1979; Hoek and Bray, 1981). The geotechnical tests showed that the material of the interface made of clay with arenite nodules and located between the silty clays (samples 3, 4, 5, 6, 11 in Table II) and the arenites has the lowest shear strength. Though this layer was not considered in the geophysical model, due to its small vertical dimension (30–70 cm), it may turn out to have a significant influence on the slope stability , as slip surfaces rooted in this layer were observed in the trenches. Therefore, in addition to the arenites, silty clays and Neogene sediments, this interface layer was included into the models used for slope stability computations.

Two types of slope stability calculations were carried out in 2D: finite element (FE) modelling with the CRISP94 code (Britto and Gunn, 1994) under static conditions and static and pseudo-static computations with Janbu's method (Janbu 1973).

8.1. Static FE Modelling

The finite element computations were carried out to study the deformability of the geological material under static conditions. The simple slope model (Figure

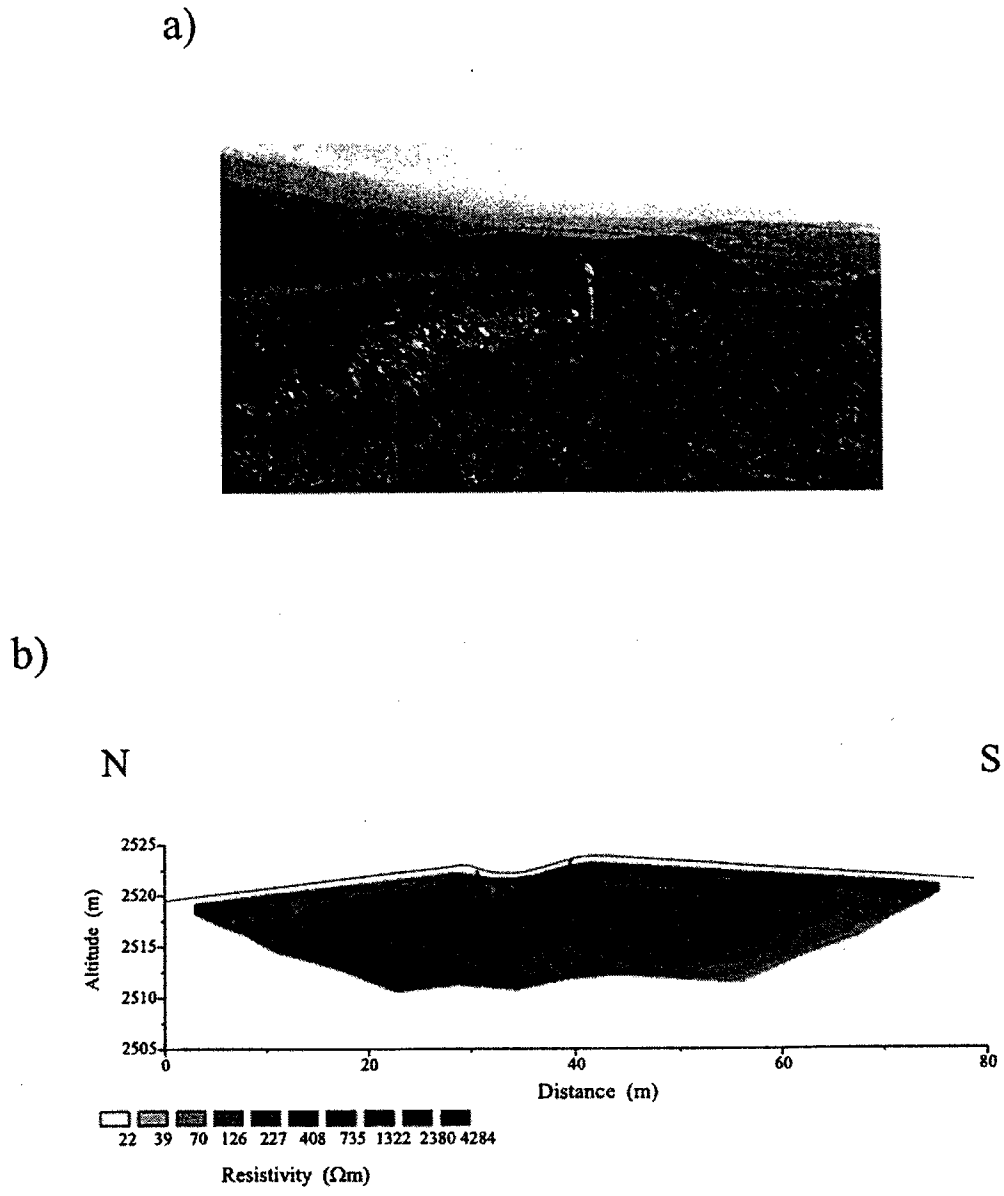

Figure 6. (a) Photograph of the graben on the crest of the Chet-Korumdy ridge. The scale is given by the 1.8 m tall person standing near to the south-facing scarp. b) Geoelectric section across the graben with interpretation of the failure geometry.

7a) used for the FE modelling corresponds to the FE section through the Chet-Korumdy ridge (Figure 2a), between the Suusamyr valley in the south and a higher dry valley north of the crest. It has been built on the basis of the Y3-section using the 3-layer model, which was extrapolated towards the south and the north, according to the morphology, the hydrological conditions and observations on outcrops. The topography of the FE model was obtained from the digital elevation model in Figure 2a representing the site conditions prior to the 1992 earthquake. The FE mesh consists of more than 1200 quadrilateral elements. The numerical calculations were conducted in the elasto-plastic domain according to the Mohr–Coulomb criterion.

TABLE II

Geotechnical parameters used for slope stability modelling: cohesion, friction angle, density of layer 1 to 3 were measured by shear tests. Range of measured values are indicated in brackets. The parameters for layer 4 and the E' values for all layers are taken from references (Philipponnat, 1979; Hoek and Bray, 1981)

Layer	Nature (sample #)	Young modulus E' (Mpa)	Cohesion c (Mpa)	Friction angle ϕ (°)	Density γ
1	Arenites	60	0.020	30	1.7
	(7, 8, 13, 14)	–	(0.000–0.035)	(26–31)	(1.59–1.76)
2	Interface	40	0.025	24	1.8
	(3, 4, 5, 6, 11)	–	(0.006–0.030)	(22–26)	(1.72–1.87)
3	Silty clays	20	0.070	25	2.0
	(1, 2)	–	(0.060–0.075)	(24–26)	(1.76–2.05)
4	Neogene sediments	1000	0.150	27	2.5

Three kinds of results are displayed in Figures 7b–7d : the horizontal displacement, the vertical displacement and the shear strain. The graph representing the horizontal displacements (Figure 7b) clearly shows that they are concentrated on the steeper southern slope as it is observed in the field. In addition, the large displacements (>0.5 m) are localised in the area where the main scarp (50 m high) developed.

The calculated vertical displacements (Figure 7b) indicate a general settlement of the ridge with a total amount of 1.6 m on the crest. In this case, the numerical results for the displacement on the crest compare well with the 2 m vertical displacement due to the graben formation (see Figure 6). Notwithstanding that the displacements related to the landslide and to the graben were induced by seismic shaking and that the calculated deformation does not take into account any former strain history of the lithologies, the static FE results approximately match with the location of the failures observed at the surface.

Figure 7d presents shear strains calculated for the FE section. Maximum strains are located inside the interface layer, induced by the low friction angle (24°, Table II). A certain amount of static displacements on the surface can probably be attributed to the deformation in this layer.

8.2. Pseudo-Static Computations

Static and pseudo-static computations were accomplished on the section shown in Figure 8a, using the Janbu's method. The pseudo-static computations allow to define a critical acceleration value for which the factor of safety is1. Considering

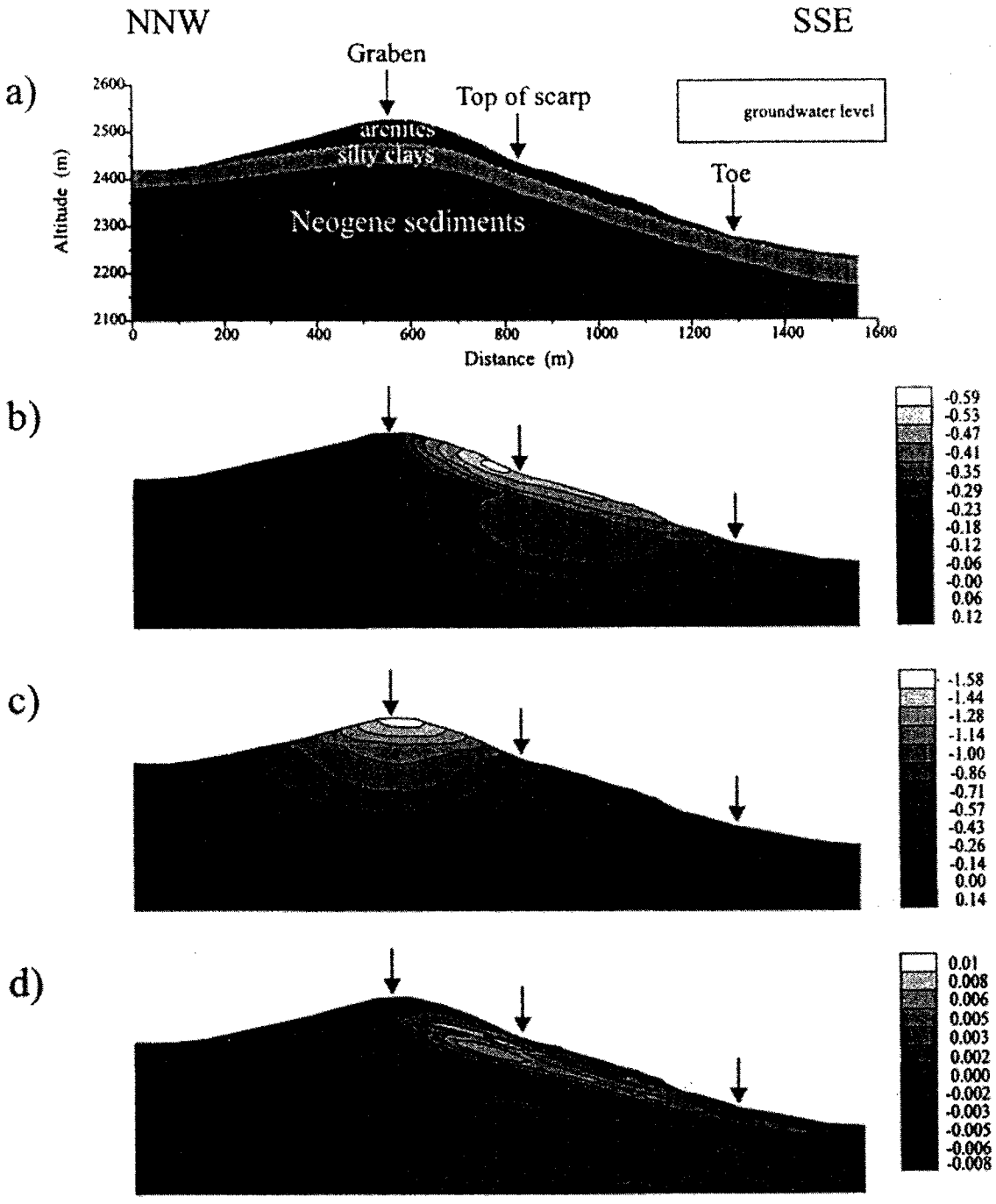

Figure 7. (a) 2D slope model used for FE computations; see Figure 2a for cross-section location. Indicated are also the location of the top of the scarp, of the landslide toe and of the graben. (b) Distribution of horizontal displacements over the section. (c) Distribution of vertical displacements. (d) Distribution of strain intensities.

this value, the displacement can be calculated according to Newmark's method (Newmark 1965). The layer geometry and the respective mechanical properties (Table II) are the same as for the FE model. By trial and error tests, the least stable slip plane was determined (Figure 8a). Its trace is analogous to the one outlined on the Figure 7d, because it runs for the most part along the interface layer between arenites and silty clays. Under static conditions, the factor of safety for this surface amounts to 1.14. To simulate the effect of an earthquake, a constant horizontal

acceleration oriented away from the slope is applied to the landslide model. Varying the acceleration value, we observe that the factor of safety becomes 1 for an acceleration of 0.05 g.

According to Newmark's method, it is possible to evaluate the theoretical displacement generated by the seismic shaking. Since no recording of the Ms = 7.3 Suusamyr earthquake is available for the investigated site, an accelerogram was simulated at 5 km from the fault rupture using the stochastic method of Boore (1996). The double-corner source spectrum of Joyner (1984) was used as source model. The stress drop was determined to 17 bars (Mellors et al., 1997) and the high frequency diminution parameter was fixed to 0.04.

The Newmark's procedure (Newmark, 1965) consists in subtracting the critical acceleration (here = 0.05 g) from all the amplitudes of the accelerogram. The resulting accelerogram is then integrated twice over time to obtain the final Newmark displacement. The basic assumptions of the method are the following : the landslide is considered as a rigid and homogeneous block, and the critical acceleration is assumed horizontal, time independent and constant over the whole landslide mass.

Notwithstanding that these hypotheses limit the application of the method to landslides with a "rigid block" structure, it may give reasonable results if interpreted correctly, even if the restrictions are not fully met (Jibson et al., 1998).

The accelerogram simulated on rock and the corresponding Newmark displacement are shown on Figures 8c and 8d. As can be seen from the accelerogram, the peak acceleration is not very high (0.14 g), mainly due to the low stress drop (usually stress drops are larger than 50 bars). As a consequence, the calculated Newmark displacement of 0.06 m is small. This value does not compare with the real displacements (of about 70 m for the debris slump alone) for different reasons. First, the Newmark displacement does not take into account post-seismic displacements and the plastic behaviour of the ground. Secondly, many factors are poorly constrained or not considered as the hydrological conditions or the change of the geotechnical parameters during the dynamical loading. Finally, site dependent amplification effects of the ground motion were not yet included.

8.3. The Site Response

In the following, special attention is paid to the site specific ground motions, which could strongly increase the displacement (Crespellani, 1996). The accelerogram shown in Figure 8c was simulated for a hard rock site exempt from any site. The actual landslide developed, however, in soft deposits, and the ground motion characteristics might be significantly different (see e.g., Bard, 1995), with amplification in a specific frequency range and increase of the duration if 2D or 3D effects are involved.

Actually, no seismological data were collected in the site and a theoretical approach is needed to evaluate these site effects. We used the method developed by Kennett (1983) to calculate the site response of a horizontally stratified medium

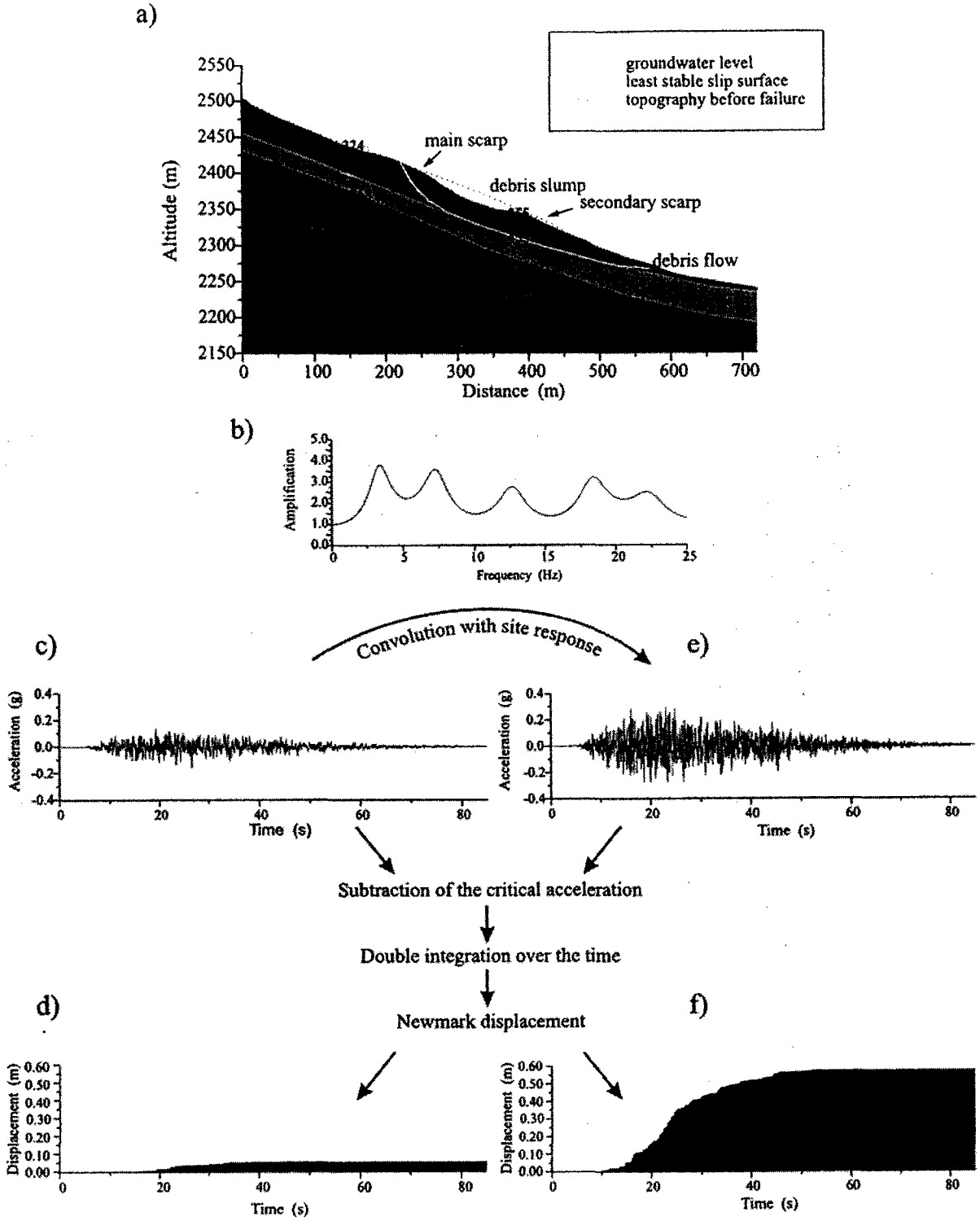

Figure 8. (a) Geological section (corresponding to section Y3 on Figure 2c) used for static and pseudo-static slope stability calculations using Janbu's method. The graph also displays the Vs models of two seismic profiles projected on the section. (b) 1D theoretical amplification for the Vs model 1 in Figure 8a (see also Table III). (c) Accelerogram obtained by stochastic simulation (Boore, 1996) of the ground motion at 5 km from the fault rupture related to the Ms = 7.3 Suusamyr earthquake. (d) Newmark displacement calculated for the accelerogram (b) and for a critical acceleration of 0.05 g. (e) Accelerogram in (c) convoluted with the 1D theoretical site response calculated for the Vs model 1. (f) Newmark displacement for the convoluted accelerogram.

TABLE III
Parameters for 1D-site response modelling (center of profile SP1, see Figure 2c)

Layer	Depth (m)	Density	S-velocity (m/s)	Qs
1	0	1.7	255	13
2	11.3	2.0	455	26
3	44.7	2.4	1350	690

(1D). This is a strong simplification, as the layer geometry is clearly 3D (Figure 4). The additional needed parameters are the S-velocity, the density and the quality factor Qs within each layer (Table III). Besides the density, which was determined from laboratory tests on samples, the two other parameters were obtained from the inversion of the surface waves generated during seismic prospecting.

The Vs models determined at the centre of the two nearest seismic profiles were projected on the section shown on Figure 8a. Figure 8b presents the amplification function calculated for the Vs-model of profile SP1, whose characteristics are shown in Table III. The convolution product between the simulated accelerogram (Figure 8c) and the amplification function is shown on Figure 8e. The accelerogram clearly exhibits larger amplitudes (PGA of 0.3 g) than the original record (0.14 g). As a consequence, the calculated Newmark displacement in Figure 8f is 10 times larger (0.6 m) than the displacement obtained on the basis of the initial recording. This result, which shows the significant influence of site effects on landslide motion, is not relevant for quantitative back-analysis purposes, because it was still obtained on the base of oversimplified assumptions. However, thanks to its simplicity, the computation of the 1D site response could be easily included in regional seismogenic landslide hazard estimates. Actually, most seismic landslide hazard studies as those realised by Jibson et al. (1998) or Miles and Ho (1999) do not take into account site effects.

9. Conclusions

In this paper, we presented the results of a geophysical survey performed in the Suusamyr valley, Kyrgyzstan. The survey including electrical tomography and refraction seismics aimed at the investigation of ground surface effects generated by the Suusamyr earthquake in 1992. During the event, tens of landslides and many surface ruptures were triggered in soft deposits along the Suusamyr valley. Our study was focused on a landslide of 0.5 to 1 $\times$ 10^6 m^3 in volume located at a distance of less than 5 km from the seismogenic fault trace. The landslide presents a complex pattern of rupture processes combining multi-rotational slumping in

the upper part and flowing downhill, which damaged the Bishkek-Osh road. The superficial materials including mainly arenites and disparate granite boulders are characterised by a high electrical resistivity ranging from about 80 Ωm to more than 1000 Ωm in very dry conditions. The seismic P-velocity is about 600 to 1500 m/s and the S-velocity about 300 to 500 m/s. The Quaternary arenite deposits are lying over Neogene sediments constituted by a succession of clay and sand layers with P-velocities of 3400 m/s and S-velocities of over 1000 m/s. Comparing morphological features and observations in two trenches with geophysical results allowed to show that the landslide mass is principally made of the arenites and that the surface of rupture is located at the contact with the underlain Neogene sediments. Although the presented geophysical methods suffer some limitations, the combined use of the two techniques allowed to define the hill structure with the presence of a thick arenite deposit covering the ridge. Convex morphologies on the slope are related to thicker accumulations of arenites that may be the heritage of old mass movements transporting the arenites from the crest downhill. Field observations, geophysical measurements and stability calculations have shown that landslide hazard is closely connected with these convex morphologies.

Using the geological and geotechnical model defined from geophysical results and laboratory tests, 2D finite element modelling in static conditions was performed. In spite of insufficiently constrained data and initial conditions, locations of theoretical maximum displacements compared well with observations of failure in the field. The application of Janbu's method leads to a factor of safety of 1.14 for the same static conditions and shows that a small horizontal acceleration of 0.05 g is required for causing the instability. The Newmark displacement calculated for a synthetic accelerogram of the 1992 Suusamyr earthquake is small (0.06 m). The influence of soft shallow deposits on the ground motion was computed using the Vs and Qs values deduced from surface wave inversion, and it was shown that site effects are a major factor increasing the Newmark displacement by a factor of 10. Even if the entire dynamic behaviour of the ground is not included here, these results highlight the need to consider the dynamic effects to asses predict the motion of a landslide during an earthquake.

Finally, this study has shown that geophysical prospecting associated with field observations and geotechnical studies turns out to be a valuable and reliable tool for investigating different aspects of instability phenomena, particularly in remote areas where classical tests (SPT, drilling, ...) are difficult to perform.

Acknowledgements

The research leading to this article was funded by the European Community (EC, DG XII contract IC15-CT97-0202). We wish to thank the KIS and GEOPRIBOR teams, students and scientists, who helped in acquiring the geophysical data.

References

Abdrakhmatov, K.Ye, Aldazhanov, S.A., Hager, B.H., Hamburger, M.W., Herring, T.A., Kalabaev, K.B., Makarov, V.I., Molnar, P., Panasyuk, S.V., Prilepin, M.T., Reilinger, R.E., Sadybakasov, I.S., Souter, B.J., Trapeznikov, Yu.A., Tsurkov, V.Ye. and Zubovich, A.V.: 1996, 'Relatively recent construction of the Tien Shan inferred from GPS measurements of present-day crustal deformation rates', *Nature* **384**, 450–453.

Avouac, J.P., Tapponnier, P., Bai, M., You, H. and Wang, G.: 1993, 'Active thrusting and folding along the northern Tien Shan and late cenozoic rotation of the Tarim relative to Dzungaria and Kazakhstan', *J. Geophys. Res.* **98**(B4), 6755–6804.

Bard, P.-Y.: 1995, 'Effects of surface geology on ground motion: recent results and remaining issues', in *Proc. of the 10th European Conference on Earthquake Engineering*, Vienna, pp. 305–323.

Bogachkin, B.M., Mishatkin, V.N., Petrosyan, A.E., Pletnev, K.G., Rogozhin, Ye.A. and Romanov, A.A.: 1993, 'Tectonic position and geologic seismologic manifestations of the focus of the Suusamyr Earthquake (Kyrgyzstan)', *Doklady* **330**, 4.

Boore, D.M.: 1996, SMSIM-Fortran programs for simulating ground motions from earthquakes: Version 1.0, *U.S. Geol. Surv., Open-File Rept. 96-80-A* 73.

Britto, A.M. and Gunn, M.J.: 1994, *Critical State Programs CRISP 90 and CRISP 94*, Vol. 3, Cambridge University.

Cobbold, P.R., Sadybakasov, E. and Thomas, J.C.: 1996, 'Cenozoic transpression and basin development, Kyrgyz Tien Shan, Central Asia', in F. Roure, N. Ellouz, V.S. Shein and I. Skvortsov (eds.), *Geodynamics Evolution of Sedimentary Basins*, Technip, Paris, pp. 181–202.

Crespellani, T., Madiai, C. and Maugeri, M.: 1996, 'Analisi di stability ... di un pendio in condizioni sismiche e post-simiche', *Rivista italiana di geotechnica* **1**, 50–61.

Dahlin, T.: 1996, '2D resistivity surveying for environmental and engineering applications', *First Break* **14**, 275–283.

Geological Map of Kirghiz SSR: 1980, *Akad. Nauk Kirghiz SSR and Ministry of Geology*, USSR, scale: 1 : 200.000.

Ghose, S., Mellors, R.J., Korjenkov, A.M., Hamburger, M.W., Pavlis, T.L., Pavlis, G.L., Mamyrov, E. and Muraliev, A.R.: 1997, 'The Ms = 7.3 1992 Suusamyr, Kyrgyzstan earthquake: 2. Aftershock focal mechanisms and surface deformation', *Bull. Seism. Soc. Am.* **87**, 23–38.

Gomez, J.M., Bukchin, B., Madariaga, R., Rogozhin, E.A. and Bogachkin, B.: 1997, 'Rupture process of the 19 August 1992 Susamyr, Kyrgyzstan, earthquake', *J. Seismology* **1**, 219–235.

Herrmann, R.: 1987, *Computer Programs in Seismology*, Vol. 6, Saint Louis University.

Hoek, E. and Bray, J.: 1981, 'Rock slope engineering', *Institution of Mining and metallurgy* 358.

Janbu, N.: 1973, *Slope Stability Computations – Embankment – Dam Engineering*, Casagrande Volume, Wiley, New York.

Jibson, R.W., Harp, E.L. and Michael, J.A.: 1998, 'A method for producing digital probabilistic seismic landslide hazard maps: An example from Los Angeles, California, Area', *U.S. Geol. Survey Open-File Report 98-113*, 1–23.

Joyner, W.B.: 1984, 'A scaling law for the spectra of large earthquakes', *Bull. Seism. Soc. Am.* **74**, 1167–1188. Geol. Survey, Prof. Paper 1511-C, Washington.

Kennett, B.L.N.: 1983, *Seismic Wave Propagation in Stratified Media*, Cambridge University Press, Cambridge.

Korjenkov, A., Bowman, D., Haselton, K. and Porat, N.: 1999, 'Recent drainage diversions under thrusting conditions in the Suusamyr valley, the Tien Shan Range, Kyrgyzstan', *Isr. J. Earth Sci.* **48**, 63–79.

Kramer, S.L. and Smith, M.W.: 1997, 'Modified Newmark model for seismic displacements of compliant slopes', *J. Geotech. and Geoenv. Eng.* **123**, 635–644.

Loke, M.H. and Barker, R.D.: 1996, 'Rapid least-squares inversion of apparent resistivity pseudosections by a quasi-Newton method', *Geophysical Prospecting* **44**, 131–152.

McCann, D.M. and Forster, A.: 1990, 'Reconnaissance geophysical methods in landslide investigations', *Engineering Geology* **29**(1), 59–78.

Mellors, R.J., Vernon, F.L., Pavlis, G.L., Abers, G.A., Hamburger, M.W., Ghose, S. and Illiasov, B.: 1997, 'The Ms = 7.3 1992 Suusamyr, Kyrgyzstan earthquake: 1. Constraints on fault geometry and source parameters based on aftershocks and body wave modeling', *Bull. Seism. Soc. Am.* **87**, 11–22.

Miles, S.B. and Ho, C.L.: 1999, 'Rigorous landslide hazard zoning using Newmark's method and stochastic ground motion simulation', *Soil Dyn. and Earthquake Engin.* **18**, 305–323.

Newmark, N.: 1965, 'Effects of earthquakes on dams and embankments', *Géotechnique* **15**(2), 137–160.

Philipponnat, G.: 1979, 'Fondations et ouvrages en terre', *Ed. Eyrolles* 402.

Reigber, C., Angermann, D., Michel, G.W., Klotz, J., Galas, R. and the CATS-team: 1999, 'New constraints on the distribution of deformation in Central Asia: GPS results covering the Tien Shan, N-Pamir and Tarim', in *Proc. of 24th General Assembly on Geophysical Research*, The Hague, 39 pp.